

The Large Scale X-ray Emission from M87

D. E. Harris¹, J. A. Biretta², and W. Junor³

¹ Smithsonian Astrophysical Observatory, 60 Garden St, Cambridge MA 02138, USA

² Space Telescope Science Institute, 3700 San Martin Dr., Baltimore, MD, 21218 USA

³ University of New Mexico, 800 Yale Blvd. NE, Albuquerque, NM, 87131 USA

Abstract. We describe asymmetrical features in a long exposure X-ray map of M87 made with the ROSAT High Resolution Imager (HRI). A bright triangular region is marked by a linear ‘spur’ along one edge. The structure of this spur suggests an interpretation of a tangential view of a shock front 18 kpc long. None of the brighter features are spatially coincident with radio or optical structures so we concur with earlier investigators that most of the emission arises from thermal processes.

1 Introduction

In addition to the strong X-ray emission (roughly circularly symmetric) from the gas associated with M87 and the Virgo cluster, asymmetric X-ray features have been known since the Einstein Observatory observations were obtained 15 years ago (Schreier, Gorenstein, and Feigelson (1982), Feigelson et al. (1987)). From these data, it was noted that the large scale X-ray emission which is asymmetric was roughly correlated with the intermediate scale radio structure, and both inverse Compton emission and thermal bremsstrahlung emission were considered as possible origins. More recently it has become clear that there is not a tight spatial correlation between radio and X-ray emissions (Böhringer et al. (1995)), and thus the inverse Compton process is not the major contributor to the observed X-rays.

In this paper, we present further information on these structures derived from an analysis of a ROSAT HRI map consisting of many monitoring observations. The effective integration time for this map is 202 ks and we are thus able to delineate weaker features with relatively high resolution. The X-ray emissions from the core and knot A in the radio jet will not be dealt with here (see Harris, Biretta, and Junor, this volume, for the latest variability data on the core and knot A).

2 Construction of the Image

The inherent spatial resolution of the ROSAT HRI is close to $5''$. However, the effective resolution can be degraded by two types of aspect (i.e. pointing) problems: the star trackers occasionally make gross errors of order $10''$ and there is often a residual error associated with the spacecraft wobble. The first type of error results in erroneous locations in celestial coordinates and is seen most often

when combining observations taken 6 months apart, although occasionally there will be an aberrant observation interval in the typical observation consisting of 10 or more intervals. The second type of error produces an ellipsoidal point response function (PRF) which can smear the $5''$ inherent PRF to something like $7''$ by $10''$. Since the current objective is to study the larger scale structures, we have not addressed these errors except for the alignment of observations.

Our monitoring program has resulted in the accumulation of 5 observations ranging from 30 to 44 ksec each, at 6 month intervals between 1995Jun and 1997Jun. To these we added the 13.9 ks HRI observation obtained in 1992Jun, resulting in a total of 202 ks. Before adding each observation, we measured the position of both the core and knot A, and shifted each observation (up to $6''$) so as to align all the data to the reference frame of the 1992Jun observation. The resulting events file is represented by the map in Fig. 1, to which we have added labels for some of the features described in section 3.

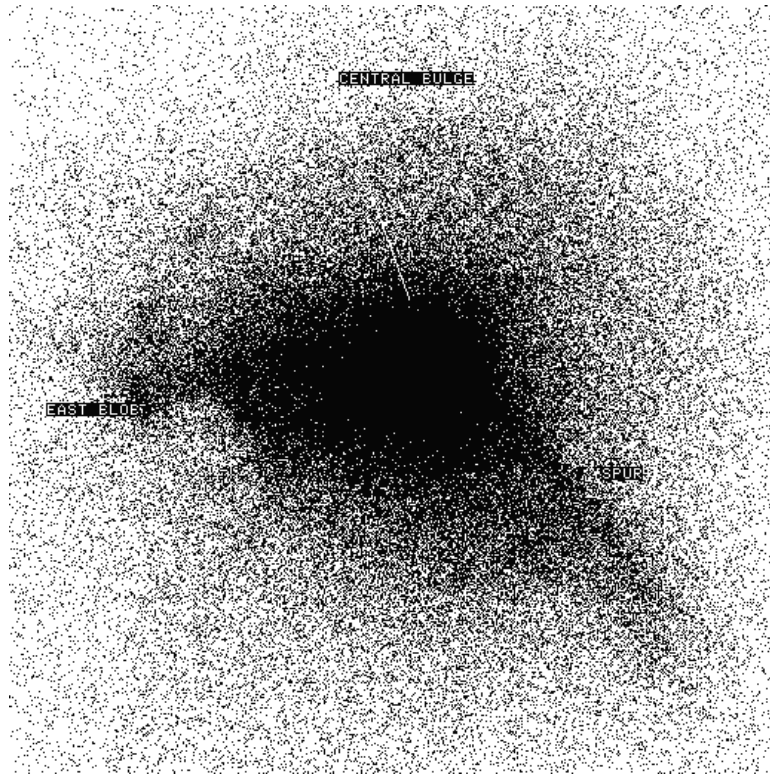


Fig. 1. The stacked image of M87 from 6 observations. Each side of the figure has a length of 256 arcsec. The core and knot A are within the burned out central region.

Since most of the asymmetrical structure occurs to the East and SW of the core, we made a radial profile only for the hemisphere between PA=240° and 60°. We chose the center for the radial profile to be $\approx 7''$ north of the core since that position appeared to be the center of the quasi circular ‘bulge’ of high brightness surrounding the core and knot A. We made no effort to fit this central bulge (radius $\approx 40''$) but found that a power law with slope of 1.10 was a reasonable fit to the brightness between 40'' and 900''. We then subtracted this power law ($1+(r/a)^{-1.1}$) from the image, adjusting the normalization until there were few negative regions. The results are shown in Fig. 2.

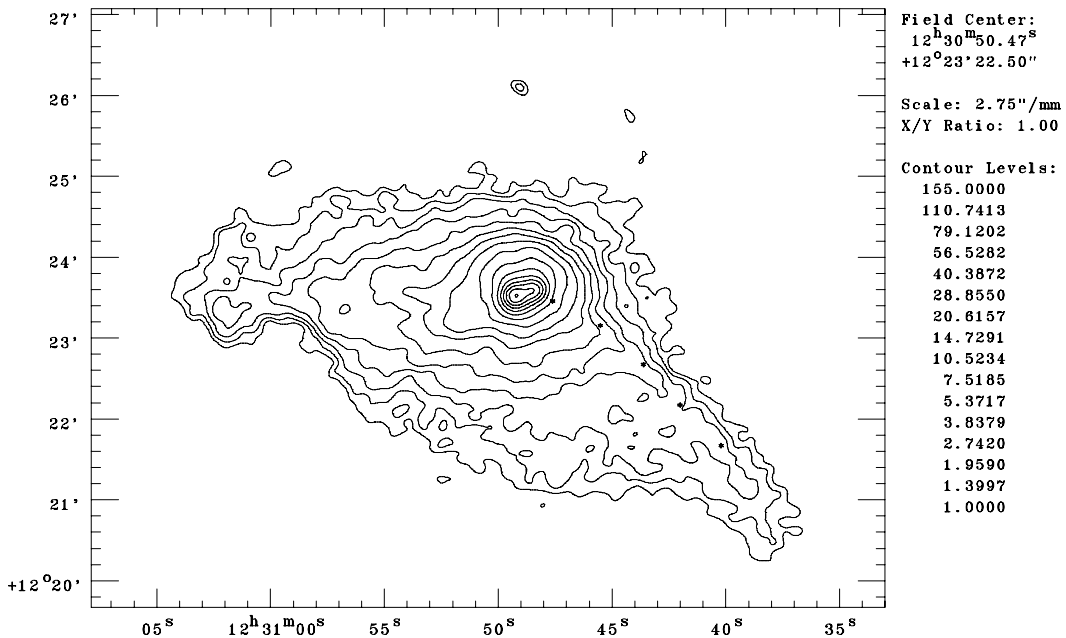


Fig. 2. The residual X-ray map after subtraction of the power law model. Contour intervals are logarithmic, starting at one count per pixel and ending at 155 counts per pixel. The pixel size is one arcsec. The map has been smoothed with a Gaussian of FWHM = 8''. The asterisks indicate measured positions along the ridge line of the SW spur.

3 Description of Discrete Features

For the most part, the following sections will describe some of the more obvious features of the X-ray distribution without a quantitative analysis. The latter subject will be addressed elsewhere.

3.1 SW spur

The most striking X-ray feature evident in Figs. 1 and 2 is the spur of emission extending from the central region $\approx 4'$ toward the south west in a slightly curved trajectory. For a distance of 16 Mpc to M87, $4'$ corresponds to 19 kpc. The NW edge is essentially unresolved but the brightness falls off more gradually behind it towards the SE. This is demonstrated in Fig. 3.

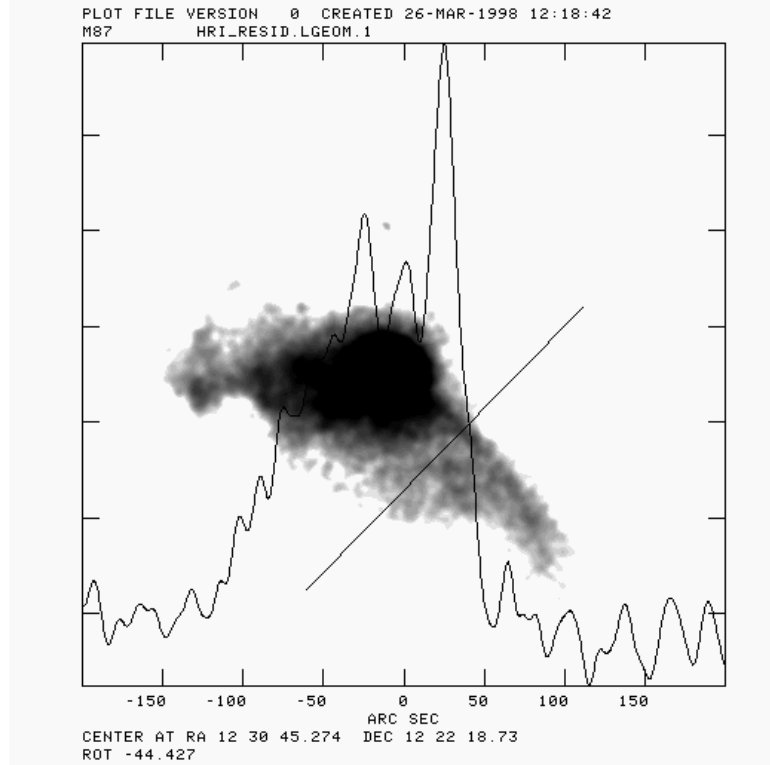


Fig. 3. A profile though the X-ray spur. Note the sharp leading edge on the right side. The X-ray map has had the model power law subtracted and was smoothed with a Gaussian of FWHM = 8''. The straight line shows the location of the measured profile.

There is no optical or radio feature corresponding to the spur, and this agrees with the results of Böhringer et al. (1995) who used a spectral analysis of the ROSAT Position Sensitive Proportional Counter observation to conclude that the asymmetric X-ray emission was thermal, but from a cooler gas than the surrounding cluster emission. However, from a preliminary hardness ratio map of our HRI data, there is some indication that the spur is actually harder than the surrounding emission.

As is often the case, it is difficult to reproduce the detail that can be obtained by visual inspection of various versions of an image. For this reason, we have added asterisks at several positions, measured by eye, of the ridge line of the spur (Fig. 2). This aid in tracing the spur closer into the core allows us to conjecture that the spur may be causally related to knot A. A possible explanation for the spur (and perhaps for much of the Eastern arm) would be that it is a tangential view of a bow shock associated with the radio jet: either knot A itself or just beyond where the jet bends sharply to the South. The excess X-ray emission which we call the spur would then come from a relatively long path length through the higher density gas compressed behind the bow shock.

A quite different scenario, but also involving a shock front, turns the argument around. If the shock is not caused by the radio jet, it would still provide a discontinuity in the ambient density, temperature, and pressure. It is just such conditions which can be the causal agent for the genesis of an internal shock in a radio jet (e.g. Hooda and Wiita (1998)); i.e. the change in external pressure is the reason that knot A exists at this location. For this scenario, the spur would be the emission from lines of sight which are tangential to the curved bow shock. From the scale of the spur and eastern arm, the most likely cause of such a shock would be the interaction of the galaxy's ISM with the ICM. Although M87 is not thought to be moving substantially with respect to the Virgo ICM, Binggeli (1998) has argued that a merger between the M87 subgroup and the M86 subgroup is in progress, and this could provide the required relative velocity between gas distributions to form a weak shock.

The chief criticism of the association between an ICM/ISM shock and knot A is that one would not expect knot A to be seen, at least in projection, near the edge of the shock. This is because the standard interpretation of the M87 jet is that it is aimed towards us, not much more than 30° to the line of sight.

3.2 Other Features Comprising the Triangular Emission Region

The brightest part of the residual image (Fig. 2) forms a roughly triangular region on the sky with the spur delineating the NW edge. The southern 'base' of the triangle is not straight, nor is it well defined; the emission falls away gradually to the south. The brightest part of the triangle aside from the core and knot A is the central bulge, a quasi circular distribution with a characteristic radius of $40''$. Extending towards the East is the 'eastern arm' which has a complex morphology. The easternmost feature in Fig. 2 is a quasi circular emission region, 'the eastern blob'. Note the sharp notch in the base of the triangle near the

eastern end of the base. It is this notch which defines the eastern blob, and it is tempting to interpret this notch as the effect of absorption. However, there is no corresponding feature on the hardness ratio map.

3.3 Lower Brightness Extended Emission

Referring now to Fig. 1, we see a lower brightness region to the north of the triangle. This region is remarkable in that it has a well defined northern boundary which is quasi circular, with a radius of $3.5'$, centered about $30''$ East of the core of M87. The circular boundary originates in the eastern blob and can be traced for over 90° . At a somewhat lower brightness, one can see extended emission below the ‘base’ of the triangle; on some displays, it appears to be somewhat striated. Finally, to the NE of the Eastern Blob, outside of the circular boundary, there is a ‘fan’ of lower brightness emission which ends near the left border of Fig. 1.

4 Acknowledgments

The work at SAO was partially supported by NASA contract NAS5-30934 and grant NAG5-2960; that at STScI by NASA grant NAG5-2957.

References

Binggeli, B. (1998): *Ringberg Workshop on M87* (Springer, Berlin, Heidelberg)
 Böhringer, H., Nulsen, P.E.J., Braun, R., and Fabian, A.C. (1995): The interaction of the radio halo of M87 with the cooling intracluster medium of the Virgo Cluster. *MNRAS* **274**, L67–L71
 Feigelson, E.D., Wood, P.A.D., Schreier, E.J., Harris, D.E., and Reid, M.J. (1987): X-Rays from the Radio Halo of M87. *ApJ* **312**, 101–110
 Harris, D.E., Biretta, J.A., and Junor, W. (1997): X-ray Variability in M87. *MNRAS* **284**, L21–L27
 Hooda, J.S. and Wiita, P.J. (1998), *ApJ* **493**, 81
 Schreier, E.J., Gorenstein, P., and Feigelson, E.D. (1982), *ApJ* **261**, 42–50